inter·noise 2023
CHIBA,GREATER TOKYO 20-23 AUGUST

Comparison of different noise sources for the simulative cabin noise assessment of an electrically propelled regional aircraft

Yannik Hüpel[1,2], Christopher Blech[2]
Institute for Acoustics, TU Braunschweig
Langer Kamp 19
38106 Braunschweig, Germany

Andrea Franco[2], Jan Werner Delfs[2]
German Aerospace Center (DLR) Braunschweig, Institute of Technical Acoustics (AS-TEA)

Bastian Kirsch[2]
Institute for Jet Propulsion and Turbomachinery, TU Braunschweig

Sabine C. Langer[2]
Institute for Acoustics, TU Braunschweig

ABSTRACT

The rising number of passengers transported by aircraft leads to more flight traffic, further increasing the environmental impact of the aviation sector. In order to combat the growing environmental impact, the Cluster of Excellence Sustainable and Energy Efficient Aviation of TU Braunschweig aims to advance research towards a climate neutral aviation industry, especially with the design of an electrically propelled short-range regional aircraft, among others. In the conscience of passengers, the focus is also shifted towards a healthy and comfortable travel experience. One of the main factors influencing these aspects is noise inside the aircraft cabin. A lower noise impact can help increase the technology acceptance and further push towards more sustainable airborne transport solutions. This contribution aims to simulatively assess and compare the sound pressure levels inside the passenger cabin of an electric propeller aircraft. The focus is laid on two of the most important noise sources: the tonal propeller excitation as well as the sound field beneath the turbulent boundary layer. The paper presents a wave-resolving FE model considering both sources and shows, which sound pressure levels can be expected, while also comparing the frequency spectra separately, therefore enabling early design changes to help reduce the cabin noise.

1. INTRODUCTION

Airborne travel is one of the most important sectors of transportation. The speed and comfort of traveling by aircraft is not only advantageous for large distances, short-range aircraft also help improve life in hard to reach regions and are therefore an indispensable part of today's world. Before the global pandemic started in 2019 commercial aircraft operations accounted for 2.4% of all global $C0_2$ emissions [1]. Of all those emissions 80% are directly linked to passenger aircraft operations [1]. Additionally, with air travel steadily recovering after the pandemic EUROCONTROL predicts an increase in aircraft travel by at least 19% until 2050 in a conservative scenario, while another scenario places the increase at 76% [2]. The data presented in the two reports showcases that one of the

[1] y.huepel@tu-braunschweig.de

[2] Cluster of Excellence SE^{2}A–Sustainable and Energy-Efficient Aviation, Technische Universität Braunschweig

contributors to $C0_2$ emissions and therefore climate change is the aviation industry. In order to fully combat climate change, it is indispensable to also make air travel sustainable and energy efficient with reaching the goal of net zero emissions by 2050. Therefore, the Cluster of Excellence "Sustainable and Energy Efficient Aviation" (SE^2A) at the TU Braunschweig has the goal of accelerating the path towards carbon neutral air travel. In order to do so, three novel aircraft designs, for the three main types of aircraft operations, have been developed. An early design of the short-range configuration, subject of this contribution, can be seen in Figure 1.
Even though carbon neutral mobility is of increasing importance to passengers, there are many other factors influencing technology acceptance of novel aircraft technologies. With increasing technological advancements passengers have been accustomed to a certain level of comfort, which is an important factor of well-being. Besides the seating arrangement and spatial configuration of the aircraft cabin, noise is the most important factor of a comfort assessment. In [3], the noise level inside the aircraft cabin is directly linked to the satisfaction, as depicted in Figure 1. It can be seen that cabin

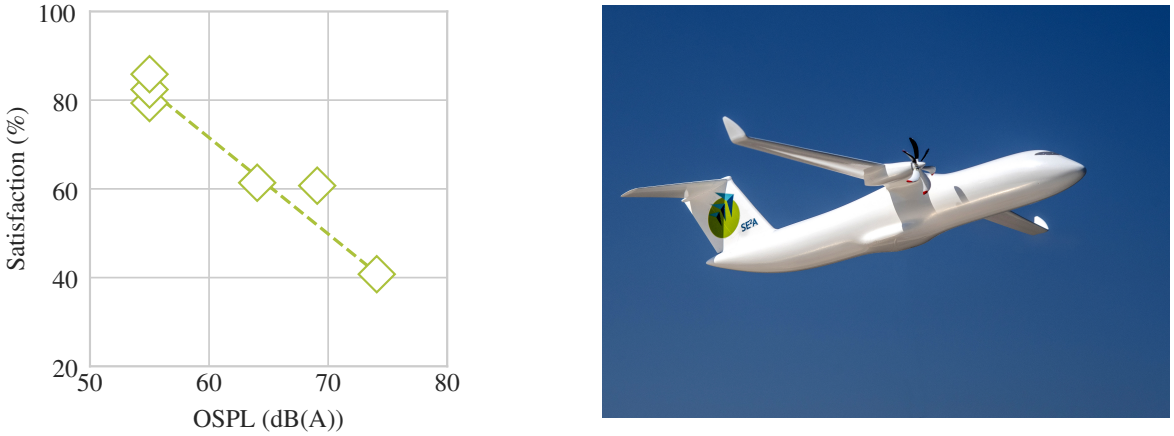

Figure 1: Left: Influence of cabin noise on comfort levels according to [3]. Right: Early design schematic of the short-range aircraft.

noise is directly linked to the satisfaction and slight increases in the sound pressure level can lead to a substantial decrease. In order to reduce CO_2 emissions it is crucial that novel aircraft designs, that can include electrically propelled machines for example, yield a certain comfort level, as to be accepted by the customer and actually used by the flight operating airlines. Therefore, it is necessary to include the noise assessment into the aircraft design process to obtain early estimates of the sound pressure level inside the cabin, so that designs can be adapted and a holistic optimization approach can be taken. It should be mentioned that operating cost and energy efficiency of course play a bigger role in aircraft design, however the acoustic aspect should not be omitted in early design phases. Since it is expensive to build prototypes for actual cabin noise experiments, the focus is laid on simulative cabin noise assessment. Here, cabin noise levels can be estimated in an early design stage and changes in the design can be adapted into the model used for the computations.
The following contribution presents an approach for the simulative cabin noise assessment of a novel electrically propelled regional aircraft. To obtain the sound pressure distribution inside the passenger cabin, the Finite-Element-Method (FEM) is used to solve a wave-resolving large-scale vibroacoustic model [4–6]. The focus of this contribution is laid on the implementation of methods that allow the examination of the resulting sound pressure level inside the cabin due to two dominant noise sources - the turbulent boundary layer (TBL) and the propeller excitation. It is shown, how pressure distributions on the aircraft's outer skin can be obtained based on CFD and CAA simulations and used as input force vector in the FEM. Finally, the resulting sound pressure level distribution inside the cabin due to TBL and propeller excitation are compared and evaluated. The developed methods yield reasonable results and allows for a simulative cabin noise assessment early on in the design process.

2. AIRCRAFT MODEL

In order to yield a sound pressure level distribution in the aircraft cabin, the wave-resolving FEM is utilized in this contribution. Before computations can be evaluated, a model has to be built. The following Section serves as an introduction to the aircraft model used in the FEM computations.
To gain insight into the sound pressure level behavior of an aircraft cabin it is sensible to evaluate the frequency response of a single or multiple points in the cabin itself. Therefore, the computations presented here are conducted in the frequency domain up to 1000 Hz. Since the computational effort of a model exponentially increases with its Degrees of Freedom (DOFs) a first simplification of the model is that only a 3 m aircraft segment is examined in this contribution. The segment is situated right before the wings, as to not have the TBL influenced by the aircraft's wings. However, even though a segment of 5 seating rows is chosen, previous evaluations by the authors show that this is sufficient for high frequencies and the gain in computational speed heavily outweighs the drawbacks of losing sound pressure level accuracy [5]. Finally, the aircraft segment model can be seen in Figure 2 and it is made up of four major domains, each influencing the resulting sound pressure level in their own way. Symmetry boundary conditions are assumed by the application of the according boundary conditions, which halves the DOFs.

The four major domains as depicted in Figure 2 are denoted by $\mathbf{\Omega_{1-4}}$. Starting with the excited airframe, $\mathbf{\Omega_1}$, the main sound transmission path will be the insulation, $\mathbf{\Omega_2}$, interior lining, $\mathbf{\Omega_3}$, and finally the cabin itself, $\mathbf{\Omega_4}$. Each of the four domains are modelled differently and are therefore explained in more detail in the following.
The **airframe $\mathbf{\Omega_1}$** is made of Carbon-Fibre-Reinforced-Polymers (CFRP) comprising an outer skin and a floor as well as frames and stringers, which are the circular and length-wise stiffeners respectively. Both are fully integrated into the airframe. For the outer skin, the floor and the stiffeners, a shell formulation (9-node quads) is used. Due to the aircraft being subjected to overpressure during cruise flight, the elements are subjected to a pre-stress accurately simulating the pressurization. For simplicity and due to a load case dimensioning not yet existing in the project, a constant thickness of 3 mm is assumed for all airframe structures, which lies in the range of a typical dimensioning for such aircraft sizes. The frames have an I-shape with a constant height of 0.1 m while the stringers are of an trapezoidal shape with a constant height of 0.05 m. The presented dimensioning will definitely influence the occurring wave lengths and therefore the cabin sound pressure level, but have little to no influence on the workflow of considering the noise sources described in Section 1. Finally, structural damping is considered by a damping loss factor $\eta_1(f)$ based on measurements on CFRP plates in [7].

The next two domains in the sound transmission path are the **insulation $\mathbf{\Omega_2}$** and the **interior lining $\mathbf{\Omega_3}$**, which make up the trim. The insulation is the filling in between the outer skin and the interior lining, where aircraft grade glass wool is used. Here, a Helmholtz domain with complex material parameters (equivalent fluid approach) is chosen in combination with the Johnson-Champoux-Allard (JCA) model [8, 9], in order to derive the frequency-dependent required complex input parameters. In addition, a limp frame extension for the JCA is considered [10]. Based on experimental data, the JCA model is shown to be suitable with certain restrictions at low frequencies [7]. In [6], the authors presented the details of also using the Biot model [11] for the insulation, but due to computational effort and a different focus the JCA model is still used in this contribution.
The interior lining is made up of honeycomb sandwiches combining a lightweight core and thin face sheets made of glass fibre reinforced plastics (GFRP) [12]. Here, 27-node hexahedrons and the above introduced 2D shell formulation (9-node quads) are assumed for the core and the face sheets, respectively. Again, based on experimental data, material parameters for both the face sheets and the core are derived in [7] and applied for the underlying studies. Structural damping is considered as well.

The area of interest, the **cabin domain $\mathbf{\Omega_4}$**, is strongly coupled to the interior linings and the floor and finally delivers the sound pressure field in the cabin. However, the cabin is coupled with non-conforming elements, further decreasing computational effort. Again, 27-node hexahedrons are considered to model acoustic waves in the cabin. Damping by passengers and seats is introduced by

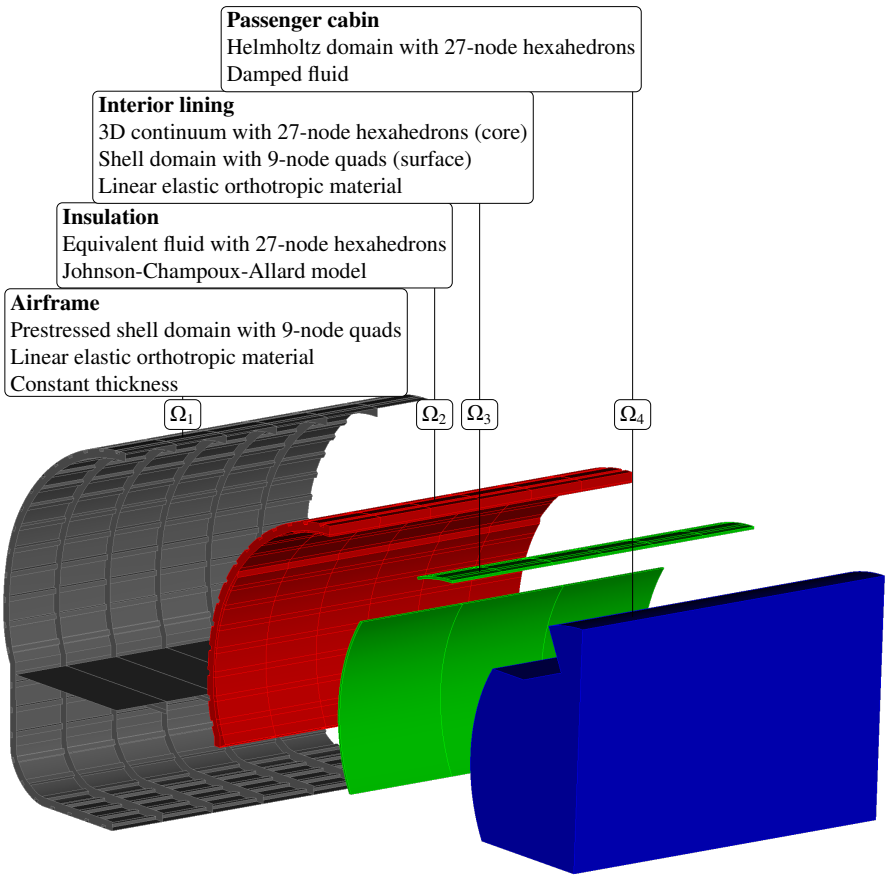

Figure 2: Vibroacoustic FE reference model comprising 2.43 mio DOFs within four major domains.

a damping loss factor $\eta_4(f)$, the determination of which has been conducted by measurements in a reverberation chamber [7].

Finally, with the application of the FEM, a final system of equations of the form

$$[\mathbf{K} - \omega^2\mathbf{M}]\mathbf{u} = \mathbf{F} \tag{1}$$

is yielded. Here $\mathbf{M}$, $\mathbf{K}$, and $\mathbf{F}$ are the mass matrix, stiffness matrix, and the force vector, respectively, which are complex-valued. The vector of unknowns is denoted by $\mathbf{u}$, while ω is the angular frequency. The size of this system is directly linked to the DOFs of the model and for the above described model the model's size is about 2.43 million DOFs. The amount of DOFs strongly depends on the examined frequency domain. In all of the different domains, the waves present have different wavelengths that are also frequency dependent, decreasing with larger frequencies. Therefore, a discretization has to be chosen that can still accurately depict the smallest waves, with at least 10 nodes per wavelength, ultimately dictating the discretization size and therefore the DOFs. Since for 1000 Hz a finer discretization than for lower frequencies is necessary, a lot of computational effort can be avoided by not only using domain-adaptive discretization as already done, but by also using frequency adaptive discretization. In Figure 3, the frequency and domain-adaptive discretization of the model is depicted.

Depending on the geometric stringer distance three different discretizations are chosen for the frequency domain, where the first can be used in computations up to 258 Hz, the second up to 578 Hz, while the finest discretization can be used up to 1000 Hz. Therefore, the sound pressure level in the whole examined frequency domain can now be evaluated efficiently, making many computations for many different variations possible.

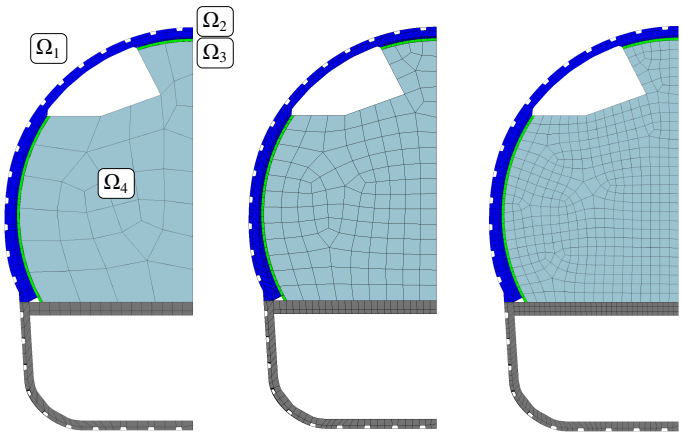

Figure 3: Frequency- and domain-adaptive fuselage meshes.

3. METHODOLOGY

This contribution aims to introduce workflows that allow for the simulative cabin noise assessment due to an TBL and propeller noise excitation. Both of these noise sources stem from an excitation of the aircraft's outer skin, meaning that the excitation leads to a change of the force vector **F** from Equation 1. Therefore, the workflow to include both noise sources in the model should ultimately aim to create a new load vector that contains the excitation of a TBL and the propeller noise. The formulation to obtain **F** due to a periodic excitation can be written as

$$\mathbf{F} = \int_{\Omega} \mathbf{N}^T p d\Omega, \tag{2}$$

where Ω is the (element-) domain, **N** denotes the ansatzfunction, and p is the excitation. Both of the considered noise sources only lead to an excitation of the aircraft's outer skin, which is modelled with 2D shell elements making p a distributed load per area. However, that means that p can be interpreted as pressure on the aircraft's outer skin, meaning that for a periodic excitation due to both noise sources the pressure amplitude as well as the phase of the excitation has to be found. Therefore, the goal of the following workflows is to implement methods that yield the pressure distribution on the airframe due to a TBL and a propeller excitation. These pressures can be used as input for the force vector computation and yield resulting sound pressure levels inside the cabin.

3.1. Turbulent Boundary Layer

As stated in [13], there are many different semi-empirical models to obtain auto spectra and wavenumber spectra on the sound pressure fields beneath the TBL. For the models, CFD data is required for the entire fuselage. The workflow developed here is adapted from [7] and deals with the computation of the pressure distribution from CFD simulation data and the following Section will give an overview of how to compute the pressures from CFD data. During the scope of the work in the SE^{2}A Cluster, three aircraft designs have been developed and the workflow will be demonstrated with the short-range regional aircraft. The input data considered in this contribution is obtained from representative cruise flight conditions for the SE^{2}A short-range aircraft design. The short-range aircraft model includes two six-bladed counter-rotating propellers, based on the TU Delft X-Prop design seen in Fig. 1.
Since a novel aircraft with an electric propulsion was developed, new CFD simulations with the Deutsche Zentrum für Luft- und Raumfahrt's (DLR) Tau were conducted and supplied. These simulations were evaluated for the cruise stage of the flight. TAU solves the Navier-Stokes equations (RANS) with a second order finite volume method [14]. For closing the RANS equations the SST model of Menter et al. [15] was used. All surfaces have been treated as fully turbulent neglecting laminar and transitional effects. To reduce the computational effort, only a half-model of the aircraft without rudder and elevator is simulated. The TAU Actuator Disc (AD) modelling option was used

to replace the propeller blades. In the AD model the computation of the disc loads is based on the Blade Element Momentum Theory, which requires data from the propeller design. The lift and drag coefficient characteristics are obtained from 2D RANS simulations for all the 23 blade sections considered. Table 1 describes the relevant parameters for the AD RANS simulation, and Figure 4 shows the dynamic pressure contours obtained from the RANS simulation.

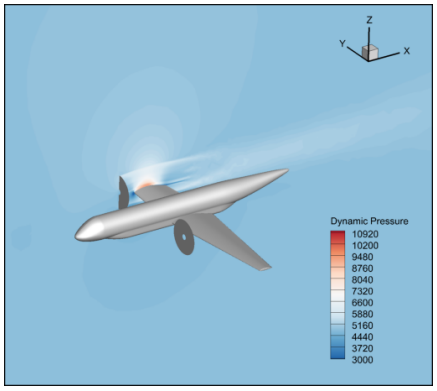

Figure 4: Contour plot of the dynamic pressure solution obtained from the AD RANS simulations.

Table 1: AD RANS Input Parameters

Input Parameter	Value
Free-stream Mach nr.	0.42
Free-stream Air Density	0.57 kgm^{-3}
Free-stream Speed Of Sound	311.0 ms^{-1}
n	13.67 s^{-1}
Propeller Blade Length	2.05 m
Thrust Single Propeller	6.4 kN
Number of Propeller Blades	6

From the simulations several slices along the main axis of the aircraft were extracted, which are similar to the slice seen around the propeller in Figure 4. For a better understanding of the post-processing of the CFD data, Figure 5 depicts the TBL thickness for the aircraft fuselage at some of the interpolation points used in the simulation.

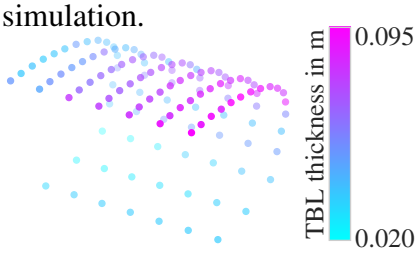

Figure 5: TBL thickness along the aircraft's length axis at certain points.

In order to fully depict the fluid behavior around the near and far field of the aircraft, many slices along the length-wise axis of the aircraft were extracted. It is important to note that these slices were extracted for different circumferential positions. For the further post-processing of the fluid parameters it is important to extract slices in such a way, that the fluid parameters along the normal of the outer skin can be extracted. This helps to simplify the computation of the pressure distribution underneath the TBL. With the slices extracted it is possible to finally start evaluating the pressure fluctuations due to a TBL.

As already mentioned in Section 3, in order to compute the excitation p, the amplitude and phase of the periodic pressure excitation is needed. Therefore, spatial and frequency-dependent information about the pressure fluctuations must be synthesized. According to [16], the autospectrum sorts the energy underneath a TBL into frequencies, meaning that the pressure amplitude can be obtained by computing the autospectrum. Using the extended Goody model [17] by Klabes [16], the autospectrum can be computed with

$$\frac{\Phi(\omega)U_e}{\tau_w^2\delta_l} = \frac{a\left(\frac{\omega\delta_l}{U_e}\right)^b}{\left[\left(\frac{\omega\delta_l}{U_e}\right)^c + d\right]^e + \left[\left(fR_T^g\right)\left(\frac{\omega\delta_l}{U_e}\right)\right]^h}, \tag{3}$$

where the coefficients $a-h$ are derived from experiments in [16]. $\Phi(\omega)$ denotes the autospectrum, U_e

the edge velocity, τ_w wall shear stress, and δ_l the TBL thickness. R_T can be computed according to

$$\frac{U_\tau^2 \delta_l}{U_e \nu}, \tag{4}$$

where U_τ is the friction velocity and ν is the kinematic viscosity. It becomes obvious, that, except for the parameters $a - g$, which were directly taken from [16], all the other parameters can be extracted from the slices of the CFD simulation. Furthermore, Figure 5 gives some insights on the behavior of the autospectrum, since the dynamic pressure greatly influences the local TBL thickness and therefore the autospectrum in itself. Since the autospectrum depends on the angular frequency ω, a direct the energy at a certain point in the frequency domain can be evaluated, therefore yielding the pressure excitation amplitude.

In order to synthesize the pressure fluctuations underneath a TBL, the sound field's dispersion characteristics are required. For the computation of stochastic sound field samples, the so-called wavenumber spectrum is applied here. Again, there are several models for the computation of the wavenumber spectrum. This contribution utilized the Efimtsov approach [18]. Generally, sound field coherence is only present in small distances on the aircraft's outer skin beneath turbulent flows. This distance is the so-called coherence length in streamwise and cross-flow direction respectively. They can be computed according to [18]

$$\begin{aligned} \Lambda_x &= \delta_l \left[\left(\frac{a_1 \mathrm{Sh}}{U_c/U_\tau} \right)^2 + \frac{a_2^2}{\mathrm{Sh}^2 + (a_2/a_3)^2} \right]^{-1/2}, \\ \Lambda_y &= \delta_l \left[\left(\frac{a_4 \mathrm{Sh}}{U_c/U_\tau} \right)^2 + \frac{a_5^2}{\mathrm{Sh}^2 + (a_5/a_6)^2} \right]^{-1/2}, \end{aligned} \tag{5}$$

respectively. Here, Sh denotes the Strouhal number and the constants a_i are also given in [18]. It is now possible to compute a so-called coherence grid introduced in [7], in which the turbulences influence each other, while there are no correlations to other grid panels. With this approach it becomes possible to practically adapt the coherence grid to create a sensible excitation of the aircraft's outer skin. For contrast to the correlated waves in grids, in [19], the so called uncorrelated plane wave method, for which comparisons are planned in future.

With the coherence grid supplying information on how the turbulence behaves over the distance of the fuselage, the question arises which waves are present in the turbulence. The approach presented in this paper uses a superposition of many plane waves exciting the coherence grid. This means that for each element in the coherence grid there is a random starting point, as to ensure that there is no correlation between two neighboring elements, and many superimposed plane waves excite the outer skin from that starting point. The wavenumbers for the waves are chosen in such a way that they depict the classical behavior as seen in [13]. The approach can be expressed as

$$p_j = \hat{p}_j \iint \Phi_{norm}(k_x, k_y, \omega) e^{i(k_x x + k_y y)} dk_x dk_y, \tag{6}$$

where k_x, k_y denote the wavenumbers in flow and cross-flow direction, respectively. $\Phi_{norm}(k_x, k_y, \omega)$ is the normalized wavenumber spectrum according to [18], which can be computed according to

$$\begin{aligned} \alpha_x &= \frac{U_c}{\omega \Lambda_x}, \\ \alpha_y &= \frac{U_c}{\omega \Lambda_y}, \\ P_1 &= 4 \alpha_x \alpha_y, \\ P_2 &= \alpha_y^2 + \left(\frac{k_y U_c}{\omega} \right)^2, \end{aligned} \tag{7}$$

$$P_3 = \alpha_x^2 + \left(\frac{k_x U_c}{\omega} - 1\right)^2,$$

$$\Phi_{norm}(k_x, k_y, \omega) = \left(\frac{U_c}{2\pi\omega}\right)^2 \frac{P_1}{P_2 P_3}.$$

Since the wavenumber spectrum contains information on which wavenumbers are present in the excitation, scaling the plane waves with the spectrum will result in a correct distribution and lessen the effort of implementation, since ranges for the respective wavenumbers can be chosen. That means, that the normalized wavenumber spectrum has to be computed and then the integral over the wavenumber ranges can be evaluated. Finally, the integral contains the superimposed scaled plane waves, meaning it contains all the information of how one single plane wave is created by all the superimposed ones and what relative amplitudes and phases they have. In a last step, the extraction of the phase of the superimposed plane wave can be used as phase information for the pressure excitation. This can be related to the FEM elements again, meaning that now for each element a pressure amplitude and phase are known, which allows for a computation of the force vector according to Equation 2. Therefore, the SPL inside the cabin due to a TBL excitation can now be computed from CFD data.

3.2. Propeller Excitation

The second noise source considered in this contribution is the sound pressure fluctuation caused by the propulsion. In the described aircraft model the propulsion consists of propellers driven by electric motors. The noise from the electric machines is omitted here, only focusing on the pressure generation due to the propeller rotations. Once again, the goal is to create a workflow that allows for simulated data to be taken into account and use them as the input for the force vector as described in Equation 2. The workflow to include the simulated propeller data in the final interior noise simulation is significantly simpler than the TBL workflow and again starts with simulations. The propeller data is supplied by the DLR, who conducted all the propeller simulations. Additionally, the CFD simulation previously described is also used as input. The propeller tonal excitation data is computed based on the CFD solution used for the TBL excitations calculation. The CFD TAU results are obtained from Actuator Disc (AD) RANS simulations, which provide the background meanflow for the Acoustic Perturbation Equations + Vortical Convection Equations (APE+VCE) system, formulated to tackle simplified as well as more complex configurations that investigate propulsion installation-related noise [20]. The propeller sources for the APE+VCE system of perturbation equations are obtained as distributed line sources of strength appropriately interpolated from the AD disc surface solution. The location of the line-distributed sources is updated at each time step, according to the propeller rotational speed [20]. The propeller model is applied in a CAA framework in the time domain, and implemented in the unstructured quadrature-free experimental Discontinuous Galerkin (DG) CAA solver DISCO++ of DLR. The rotating straight line sources are defined in the plane centered at the AD location of the CFD simulations. Approximately three complete revolutions of the line source are simulated. More details can be found in [20]. The result is a pressure field on the aircraft's outer skin over different points in time. To better illustrate the propeller simulation, Table 2 summarizes the CAA simulations input parameters. Figure 6 shows the results obtained in terms of contour plots of the pressure fluctuations, with isosurfaces of Q-Criterion superimposed illustrating the modelled blade tip vortices.

Figure 6 clearly shows that the pressure maxima propagate along the aircraft's outer skin, therefore also traveling length-wise along the airframe. This makes the approach of modelling waves to include the pressure fluctuations unavoidable. However, the supplied data is still in time domain and since frequency responses of the cabin are of interest in the cabin noise simulations, the propeller data has to be transformed into the frequency domain by using a Fast-Fourier-Transform (FFT) algorithm. Additionally, the data supplied is dimensionless and the dimensioning has to be included also.
Finally, this leads to frequency pressure data due to the propeller excitation. Since a regular FFT has been conducted the pressure data in frequency domain is complex, meaning that amplitude and phase

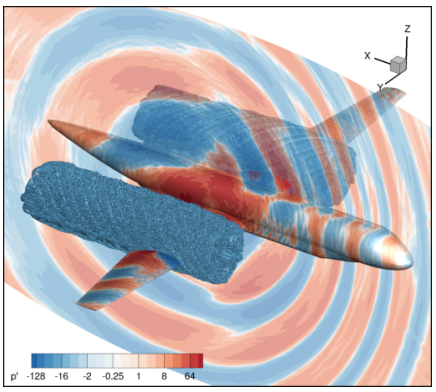

Figure 6: Contour plot of p' in Pa with Q-Criterion iso-surfaces superimposed.

Table 2: CAA Input Parameters

Input Parameter	Value
Free-stream Mach nr.	0.42
n	13.67 s^{-1}
Propeller Blade Length	2.05 m
Thrust Single Propeller	6.4 kN
Farf. Tetra Cell Size	0.2072
Refin. Tetra Cell Size	0.02072
Number of Time Steps	220,000
Time Step Size	0.0001

can easily be extracted to be included in the plane wave approach as described in the previous section. This allows the evaluation of the cabin noise due to a propeller excitation.
However, in a final step both noise sources should be considered together. Therefore, the question arises as to how to get a combined excitation, but since both phenomena are modelled to be plane waves along the aircraft's outer skin, a simple superposition of both amplitude and phase can be computed. Again, this yields one combined plane wave per element which can be used in the computation of the force vector according to Equation 2. Lastly, it should be mentioned here, that the FEM nodes do not always overlap with the nodes used in the CFD or CAA simulation, meaning that an interpolation has to be utilized, in order to obtain the needed input data at any given point. Since both the CFD and CAA simulation use a very fine mesh, a nearest neighbor interpolation can be employed efficiently.

4. RESULTS

The following section serves to show that with the workflow described in the previous section it is possible to obtain physical sound pressure levels of the aircraft's cabin. Therefore, the mean squared sound pressure levels inside the cabin will be evaluated. The mean squared is chosen as to give an energy-based indication of the sound pressure level and mean across the cabin itself. However, due to the FEM being used, it is possible to evaluate the sound pressure at every point in the cabin. The evaluation at the seats where the passenger's heads would be feasible as well in order to gain more insights into the final comfort level. Due to many uncertainties in the simulations the mean squared sound pressure is a good indicator for this contribution. In Figure 7, the mean squared sound pressure due to the TBL excitation with the workflow described above is shown. Since the TBL excitation is a stochastic source, the noisy frequency response has been expected. However, it is also expected that at higher frequencies not as much energy is transmitted into the system, since the autospectrum drops off quite fast with increasing frequency. This can be seen in Figure 7. The frequency response characteristics are comparable to white noise, but still some resonances of the system can clearly be observed. Especially in lower frequencies, there is a lot of energy transmitted into the aircraft, which is to be expected when examining the autospectrum. The overall SPL of about 65 dB is also physically reasonable, meaning that the established workflow can be used to get a first indication of the SPL due to a TBL excitation. Since only half of the fuselage was modeled here and a symmetry boundary condition was used, due to the TBL excitations being uncorrelated 3 dB have to be subtracted from the final result [7], because of the superimposing of the signals. More important, however, is the fact that with the workflow, relative studies of the influence of dimensioning and design on the interior aircraft noise can be conducted.

In order to verify the workflow of including the propeller excitations in the presented model, it

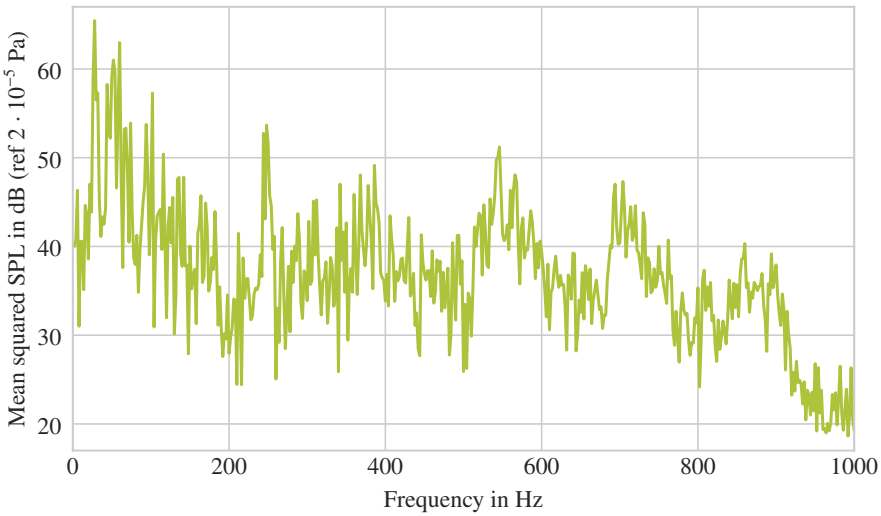

Figure 7: Mean squared sound pressure inside the aircraft cabin due to TBL excitation.

is sensible to compare the cabin noise due to a sole TBL excitation with the interior noise generated by the combined excitation of both TBL and propeller, because it is expected that the propeller noise will be highly tonal. This means that at the Blade Passing Frequency (BPF) and the multiples thereof, an even bigger amount of energy should be transmitted into the system, leading to higher SPLs inside the cabin. With the given propeller data the BPF is around 80 Hz. Here, higher peaks in the response should be expected. In Figure 8, the comparison of the previous Figure and the SPL due to the combined excitation is depicted. Again, the propeller excitation on both sides are uncorrelated which has been accounted for by modifying the symmetry boundary condition.

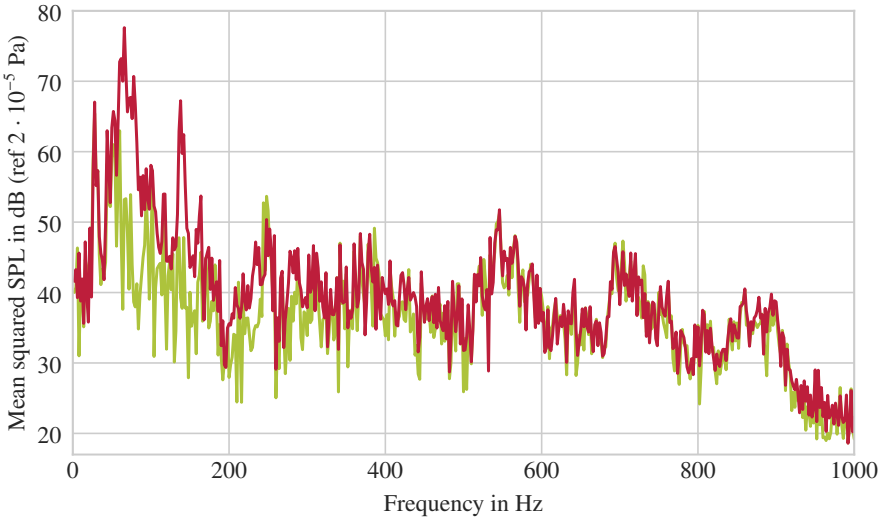

Figure 8: Comparison of the mean squared SPL of the TBL excitation (green) and a combined TBL and propeller excitation (red).

It can clearly be observed that around the BPF there is a higher peak, meaning that the propeller excitation is indeed highly tonal and behaving as expected. Additionally, the first multiple of the BPF also leads to a high peak in the SPL supporting the fact that also the harmonics of the BPF have a higher energy transmission into the system. This leads, to the assumption that the obtained results are physical and the established workflow can be used to predict the interior cabin noise of a novel aircraft. Still there are some drawbacks to the elaborated approach, but the workflow should be used as a first indicator of interior noise to shift the aircraft design towards an even more holistic approach, where acoustics and comfort can also be considered from an early design phase.

5. SUMMARY AND CONCLUSION

This contribution presented an approach to include broadband and tonal noise sources in simulations for the evaluation of interior aircraft cabin noise of an electrically driven regional propeller aircraft. Since the designs are not final and no prototypes have been built, the approach aims to assess the cabin noise simulatively based on CFD and CAA simulations' input. The contribution shows one possible way to include these processes in the simulation chain and evaluate the generated cabin noise and use the computations for design changes, enabling a more holistic design approach, where acoustics could also be considered in early design phases.

Important TBL parameters are extracted from numeric CFD simulations, which allow the computation of the pressure fluctuations beneath the TBL. The overall approach being that many small turbulences are correlated in certain areas of the aircraft's outer skin, those lengths being the coherence lengths. The presented approach creates a coherence grid in which the TBL is modelled to create a pressure wave. Since random starting points in the coherence grid elements are chosen for the plane waves, the waves from different grids do not correlate with each other. The amplitude of the pressure wave is computed with the autospectrum that sorts the energy underneath a TBL into frequencies. The phase of the wave is computed with the superposition of many different plane waves that are scaled with the normalized wavenumber spectrum, which contains information on which waves are actually present in the TBL. This leads to one superimposed pressure wave per coherence grid element that can be used as element load for the FEM element. The presented methods leads to physically meaningful results and good estimates of the SPL are obtained.

The propeller-induced tonal excitations have been included based on a simplified, non-empiric physical principles-based approach for the prediction of installed rotor noise. Time history of pressure fluctuations on the aircraft's outer skin was supplied, which allowed the inclusion of these excitations by means of a FFT computation.

The presented workflow leads to qualitatively meaningful SPL estimates to be used in early design stages of an aircraft, and can be integrated in an automatized simulation chain, allowing the inclusion of acoustics early on in the iterative process. However, the presented approach also has its drawbacks. Since the coherence grid aims to have no correlation between coherence grid elements a sudden change of the wave's phase can occur and skew the results. Especially for challenging geometries, as in the presented aircraft with battery box, the implementation of the coherence grid can also lead to further inaccuracies. Additionally, due to the excitations being uncorrelated, a lower SPL due to destructive interference should not happen, which means that in the future an energy-based combination approach of the two sound sources could improve the presented workflows. Therefore, the presented approach is seen as the start of further improving the inclusion of realistic loading in automatic simulation chains for cabin noise assessment.

Ongoing work at the Institute for Acoustics aims to validate several other models of pressure fluctuations beneath a TBL by conducting wind tunnel experiments. Furthermore, the workflow and the model are both subject to uncertainties, may they be of modelling or material kind. These uncertainties can be included in the simulations itself, leading to a more robust estimation of the cabin's SPL. With all those simulations it is also important to keep computational effort as low as possible, which is why the authors continuously work on surrogate modeling for large-scale systems.

ACKNOWLEDGEMENTS

We acknowledge the funding by the Deutsche Forschungsgemeinschaft (DFG, German Research Foundation) under Germany´s Excellence Strategy – EXC 2163/1 – Sustainable and Energy Efficient Aviation – Project-ID 390881007.

References

1. Brandon Graver, Kevin Zhang, and Dan Rutherford. CO2 EMISSIONS FROM COMMERCIAL AVIATION, 2018. 2019.
2. EUROCONTROL. Aviation Outlook 2050.

3. Henning Scheel and Pierre Lempereur. Next generation Aircraft-A challenge for Interior Acoustics Developments. 2016.
4. Christopher Blech, Christina K. Appel, Roland Ewert, Jan W. Delfs, and Sabine C. Langer. Numerical prediction of passenger cabin noise due to jet noise by an ultra–high–bypass ratio engine. *Journal of Sound and Vibration*, 464:114960, 2020.
5. Christopher Blech, Christina K. Appel, Roland Ewert, Jan W. Delfs, and Sabine C. Langer. Wave-Resolving Numerical Prediction of Passenger Cabin Noise Under Realistic Loading. In Rolf Radespiel and Richard Semaan, editors, *Fundamentals of High Lift for Future Civil Aircraft*, volume 145 of *Notes on Numerical Fluid Mechanics and Multidisciplinary Design*, pages 231–246. Springer International Publishing, 2021.
6. Christopher Blech, Yannik Hüpel, and Sabine Langer. Modelling Aspects for High-fidelity, Large-scale Aircraft Cabin Noise Simulations. In *von Estorff, Lippert (Ed.) 2023 – Fortschritte der Akustik, Proceedings of DAGA 2023*, pages 561–564.
7. Christopher Blech. *Wave-resolving aircraft cabin noise prediction*, volume 2022,1 of *Schriften des Instituts für Akustik*. Shaker, Düren, 2022. doi.org/10.2370/9783844087017.
8. David Linton Johnson, Joel Koplik, and Roger Dashen. Theory of dynamic permeability and tortuosity in fluid-saturated porous media. *Journal of Fluid Mechanics*, 176(-1):379, 1987.
9. Yvan Champoux and Jean-F. Allard. Dynamic tortuosity and bulk modulus in air–saturated porous media. *Journal of Applied Physics*, 70(4):1975–1979, 1991.
10. R. Panneton. Comments on the limp frame equivalent fluid model for porous media. *Journal of the Acoustical Society of America*, 122(6):EL217–EL222, 2007, 2007.
11. Noureddine Atalla, Raymond Panneton, and Patricia Debergue. A mixed displacement-pressure formulation for poroelastic materials. *The Journal of the Acoustical Society of America*, 104(3):1444–1452, 1998.
12. S. Ebnesajjad. *Handbook of adhesives and surface preparation: technology, applications and manufacturing*. William Andrew, 2010.
13. Alexander Klabes. *Aircraft Fuselage Vibration Excitation by Turbulent Boundary Layer Flow in Cruise*. Dissertation, Deutsches Institut für Luft- und Raumfahrt e.V., 2017.
14. D. Schwamborn, T. Gerhold, and R. Heinrich. The DLR TAU-Code: Recent applications in research and industry, 2006.
15. F. Menter, Kuntz, M., Langtry, R., K. Hanjalic, Y. Nagano, and M. J. Tummers. Ten Years of Industrial Experience with the SST Turbulence Model. *Turbulence, heat and mass transfer 4*, pages 625–632, 2003.
16. Alexander Klabes, Christina Appel, Michaela Herr, and Sören Callsen. Fuselage Excitation During Cruise Flight Conditions: A New CFD Based Pressure Point Spectra Model. 2016.
17. Michael Goody. Empirical Spectral Model of Surface Pressure Fluctuations. *AIAA Journal*, 42(9):1788–1794, 2004.
18. B. M. Efimtsov. Characteristics of the field of turbulent wall pressure fluctuations at large Reynolds numbers. *Soviet Physics-Acoustics (Sov Phys Acoust)*, 28:289–292, 1982.
19. Laurent Maxit. Simulation of the pressure field beneath a turbulent boundary layer using realizations of uncorrelated wall plane waves. *The Journal of the Acoustical Society of America*, 140(2):1268, 2016.
20. Andrea Franco, Michael Moessner, Roland Ewert, and Jan Delfs. Fast Non-Empiric Tonal Noise Prediction Model for Installed Propulsors. In *28th AIAA/CEAS Aeroacoustics 2022 Conference*, Reston, Virginia, 2022. American Institute of Aeronautics and Astronautics.